JACS
JOURNAL OF THE AMERICAN CHEMICAL SOCIETY
pubs.acs.org/JACS

Article

Controllable Active Intermediate in CO_2 Hydrogenation Enabling Highly Selective *N,N*-Dimethylformamide Synthesis via *N*-Formylation

Jieyun Zhang,[‖] Guanna Li,[‖] Jin Xie, Yang Hai, Weiming Wan, Haotian Sun, Bin Wang, Xiaojing Wu, Jiannian Cheng, Changxin He, Wei Hu, Ying Zhang, Zelong Li,* and Can Li*

Cite This: https://doi.org/10.1021/jacs.4c12503

Read Online

ACCESS | Metrics & More | Article Recommendations | Supporting Information

ABSTRACT: *N,N*-Dimethylformamide (DMF) is a widely used solvent, and its green and low-carbon synthesis methods are in high demand. Herein, we report a new approach for DMF synthesis using a continuous flow reaction system with a fixed-bed reactor and a ZnO-TiO_2 solid solution catalyst. This catalyst effectively utilizes CO_2, H_2, and dimethylamine (DMA) as feedstocks, demonstrating performance with 99% DMF selectivity and single-pass DMA conversion approaching thermodynamic equilibrium. Moreover, the catalyst demonstrates good stability, with no signs of deactivation over 1000 h of continuous operation. The key to superior activity lies in the synergetic effect of the Zn and Ti sites, which facilitates the formation of active formate species. These species act as crucial intermediates, reacting with DMA to produce DMF. Importantly, the slow hydrogenation kinetics of the formate species prevent the formation of CH_2O* species, thereby suppressing the formation of the undesired byproduct, trimethylamine. This work underscores the potential of kinetically controlling active intermediates in CO_2 hydrogenation to prepare high-value-added chemicals by coupling them to platform molecules. It presents a promising strategy for the efficient utilization of CO_2 resources and offers a valuable solution for large-scale DMF synthesis.

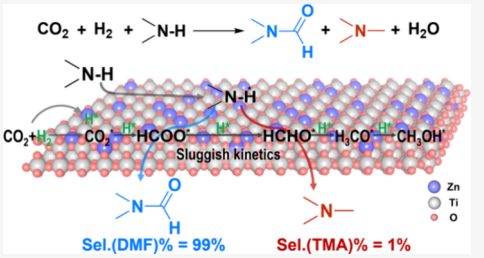

INTRODUCTION

N,N-Dimethylformamide (DMF) holds a prominent position in the global chemical market due to its versatility, serving not only as a popular solvent but also as a versatile and multipurpose reagent in various synthetic processes.[1] In the current industry, DMF is produced through the reaction of DMA with carbon monoxide (CO), catalyzed by sodium methoxide ($NaOCH_3$) in a methanol solution. However, this method generates solid waste due to the use of $NaOCH_3$, causing significant environmental concerns. In the 1970s, an environmentally sustainable pathway was developed, replacing CO with CO_2 hydrogenation by using Ir complexes, achieving a maximum turnover number (TON) of 1200.[2] This discovery spurred decades of research to improve the catalytic activity of metal complexes,[3,4] resulting in the employment of various precious metals and different ligands capable of producing DMF, with the TON increasing by 3 orders of magnitude.[5−10] Meanwhile, nonprecious metal complexes, which are highly desirable, were also developed for DMF synthesis.[11−13] Unfortunately, these nonprecious metal complexes exhibit lower activity compared to their precious metal counterparts. Additionally, separating and reusing homogeneous catalysts remain challenging.

Although heterogeneous catalysts have been developed for DMF synthesis in batch reactions, they still rely on noble metals such as Pd,[14−16] Ir,[17] and Ru.[18] This reliance limits their large-scale application due to the high cost and scarcity of these metals. Recently, the Cu/ZnO catalyst has shown a high DMF yield but requires high pressure (12 MPa) in batch reactions, posing practical challenges.[19] Conversely, the $CuAlO_x$ catalyst shows low DMF selectivity with significant formation of the byproduct trimethylamine (TMA). However, covering nano-Cu particles with nitrogen-doped layered carbon can significantly enhance DMF selectivity.[20] Furthermore, constructing Cu_2O/Cu interface active sites has been demonstrated to improve the selectivity of DMF over the $CuAlO_x$ catalyst.[21] Nevertheless, making the controllable synthesis of DMF while suppressing TMA formation remains a significant challenge, thereby limiting their large-scale application. Additionally, Cu-based catalysts face rapid deactivation due to water produced during CO_2 hydrogenation, which accelerates the sintering of the Cu active component.[22] Recycling and regenerating catalysts in batch reactions also increase energy consumption and costs.

Received: September 9, 2024
Revised: December 11, 2024
Accepted: December 11, 2024

https://doi.org/10.1021/jacs.4c12503
J. Am. Chem. Soc. XXXX, XXX, XXX−XXX

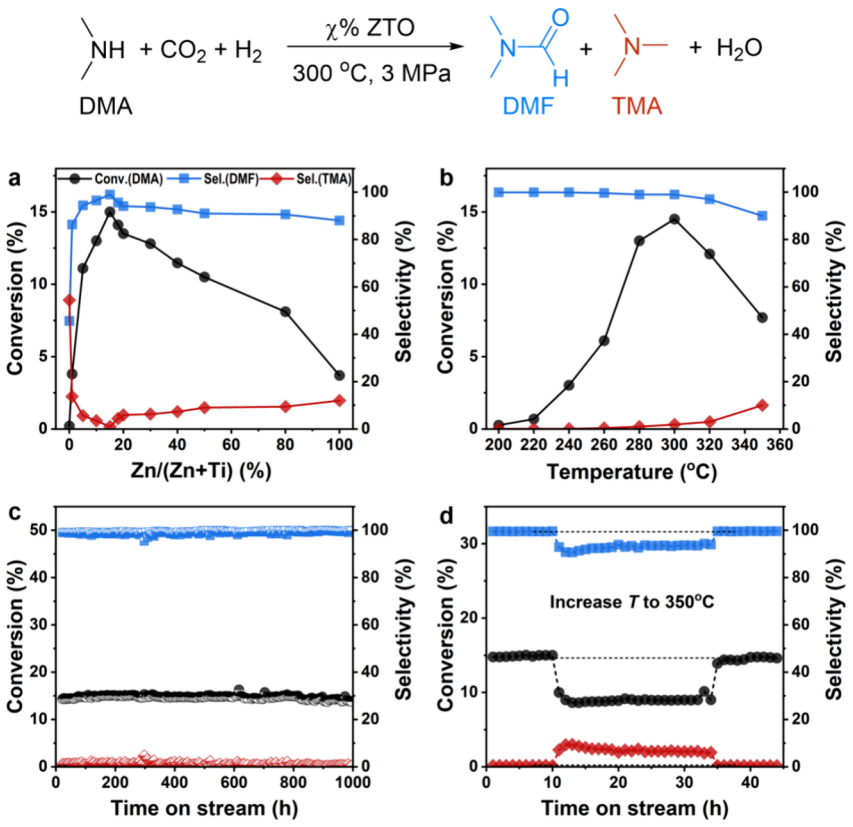

Figure 1. (a) Dependence of catalytic performance at 300 °C on the Zn/(Zn + Ti) molar ratio. (b) Catalytic performance at reaction temperatures from 200 to 350 °C. (c) Catalyst stability test in 1000 h. (d) Catalyst stability to annealing. Reaction conditions: 3.0 MPa, H_2/CO_2 = 3:1, 300 °C, GHSV = 60,000 mL/(g·h), LHSV = 5.0 h^{-1}, using a tubular fixed-bed reactor with the 15% ZTO catalyst.

Consequently, there is a pressing need to develop an efficient catalyst capable of controllable DMF synthesis through CO_2 hydrogenation with high DMF selectivity and stability under continuous fixed-bed reactor conditions to meet the requirements of large-scale production.

Here, we report a ZnO-TiO_2 solid solution catalyst that enables a highly efficient and continuous flow reaction system with a fixed-bed reactor for DMF synthesis utilizing CO_2, H_2, and DMA. This catalyst achieves a DMF selectivity of 99% at a single-pass DMA conversion of 15% under reaction conditions of 3 MPa and 300 °C, demonstrating excellent stability and making it promising for the industrial-scale DMF synthesis. The synergistic effect of Zn and Ti sites facilitates the formation of formate species, which are crucial intermediates that react with DMA to form DMF. Additionally, the slow hydrogenation kinetics of the formate species effectively hinders the formation of the side-product TMA. Moreover, this catalyst is also effective for the synthesis of *N*,*N*-diethylformamide (DEF) and *N*,*N*-dipropylformamide (DPF) with a selectivity of 99% through CO_2 hydrogenation coupled with diethylamine (DEA) and dipropylamine (DPA), respectively.

RESULTS AND DISCUSSION

A series of ZnO-TiO_2 catalysts with varying molar percentages of ZnO were prepared using a coprecipitation method. These ZnO-TiO_2 catalysts, with an atomic ratio of χ% Zn in Zn and Ti (Zn/(Zn + Ti)), are referred to as χ% ZTO. The catalytic activity for the *N*-formylation of DMA through CO_2 hydrogenation was investigated, as illustrated in Figure 1. TiO_2 exhibits very low activity in DMF synthesis. It is worth noting that the introduction of ZnO into TiO_2 significantly enhances both the DMA conversion and DMF selectivity. The optimal performance is achieved at a Zn/(Zn + Ti) atomic ratio approaching 15%, resulting in a DMA conversion of 15% and a DMF selectivity of 99% (Figure 1a). Meanwhile, the CO_2 conversion is up to 3.0% with selectivities for DMF, TMA, and CO of 93, 1, and 6% according to CO_2 conversion, respectively (Figure S1). In the absence of DMA, the CO_2 conversion is only 1.1%, displaying methanol and CO selectivities of 90 and 8%, respectively (Figure S2). In comparison, ZnO alone displays a DMA conversion of only 4%. Notably, the catalytic activity of 15% ZTO is three times that of physically mixed ZnO and TiO_2 with the same Zn/Ti molar ratio (Figure S3).

Figure 1b shows that as the reaction temperature increases, the DMA conversion initially rises and then falls, accompanied by a decrease in DMF selectivity. The maximum DMA conversion of 15% is attained at a reaction temperature of 300 °C, with DMF selectivity reaching 99%. As the liquid space velocity increases, DMF selectivity remains constant, while the space-time yield (STY) of DMF significantly improves, reaching up to 1.4 kg/(kg_{cat}·h) (Figure S4). This STY of DMF is higher than that achieved with a batch reactor (Table S1). Additionally, as the space velocity of CO_2/H_2 increases, the DMF selectivity remains at 99% (Figure S5).

The 15% ZTO catalyst exhibits no deactivation in the *N*-formylation of DMA through CO_2 hydrogenation, maintaining consistent DMF selectivity over 1000 h on stream (Figure 1c). Stability is a critical concern in CO_2 hydrogenation reactions,

https://doi.org/10.1021/jacs.4c12503
J. Am. Chem. Soc. XXXX, XXX, XXX−XXX

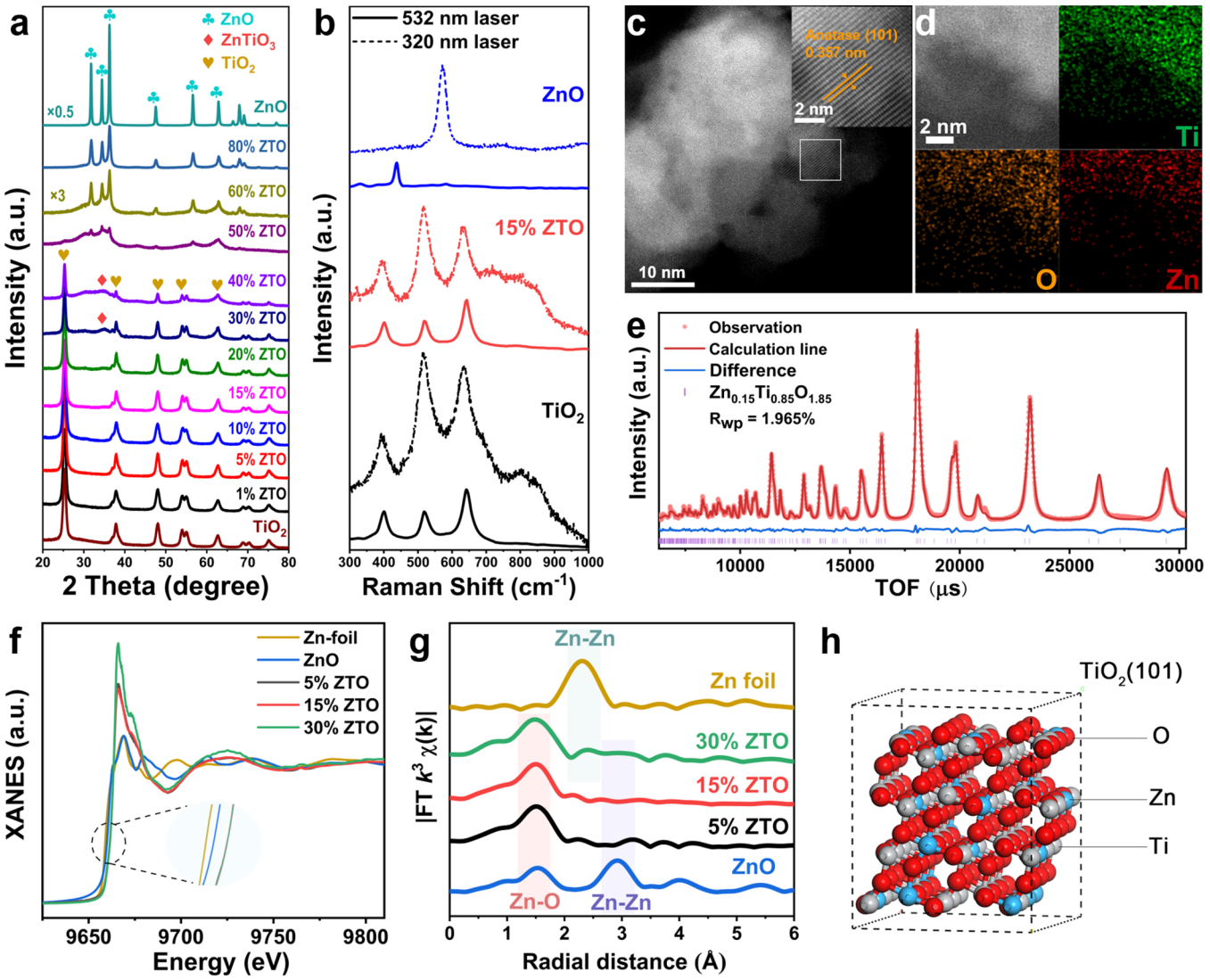

Figure 2. (a) XRD patterns of ZnO, TiO_2, and χ% ZTO. (b) Raman spectra of ZnO, ZTO, and TiO_2 with 320 and 532 nm lasers. (c) High-resolution transmission electron microscopy and (d) element distribution of 15% ZTO. (e) Neutron diffraction spectra of the 15% ZTO catalyst. (f) Zn K-edge XANES spectra for χ% ZTO, ZnO, and Zn foil. (g) Fourier-transform spectra from the extended X-ray absorption fine structure at the Zn K-edge of χ% ZTO, ZnO, and Zn foil. (h) Schematic description of the 15% ZTO solid solution catalyst model.

as many supported metal catalysts are prone to deactivation at elevated temperatures due to the sintering effect. To further explore the thermal stability of the 15% ZTO catalyst, the reaction temperature was raised from 300 to 350 °C, maintained for 24 h, and subsequently reduced back to 300 °C. No deactivation is observed after this annealing treatment (Figure 1d). Consequently, the high stability and performance of the 15% ZTO catalyst in the direct conversion of DMA through CO_2 hydrogenation position it as a viable candidate for industrial processes, demonstrating superiority over supported metal catalysts.

X-ray diffraction (XRD) patterns confirm that TiO_2 and ZnO exhibit the anatase (PDF #21-1272) and hexagonal phases (PDF #36-1451), respectively (Figure 2a). When ZnO is doped into TiO_2 with a ZnO content below 30%, the ZTO primarily exhibits the anatase phase, and the ZnO phase is not detected. The XRD pattern from the (101) spacing of TiO_2 shifts to a lower angle when the Zn concentration is increased from 1 to 30% (Figure S6). This shift indicates the formation of a ZnO-TiO_2 solid solution involving the replacement of Ti atoms within the anatase lattice by Zn. Additionally, new small peaks centered at 35° are observed for 30 and 40% ZTO, which can be attributed to the cubic phase of $ZnTiO_3$ (PDF #39-0190). This suggests the coexistence of both $ZnTiO_3$ and ZnO-TiO_2 solid solution for 30 and 40% ZnO-TiO_2. With an increase in Zn content to 50%, the anatase phase of ZTO and the $ZnTiO_3$ structure disappear, replaced by the presence of the ZnO hexagonal phase. These peaks assigned to the ZnO phase continuously increase as the Zn content reaches 60 and 80%.

Raman spectroscopy using 320 and 532 nm laser sources was employed to detect phases from the skin layer to the bulk of the χ% ZTO catalyst (Figure 2b and Figure S7). The phase near the skin layer is sensitively detected by UV Raman spectroscopy with a 320 nm excitation laser. The appearance of Raman peaks at 400, 519, and 643 cm^{-1} indicates that the skin layer of TiO_2 is in the anatase phase.[23] For ZTO with 1−20% Zn, the Raman peaks are similar to those of TiO_2, showing the anatase phase. When the ZnO content is increased from 20 to 30%, the spectrum evolves slightly, showing an additional peak

https://doi.org/10.1021/jacs.4c12503
J. Am. Chem. Soc. XXXX, XXX, XXX−XXX

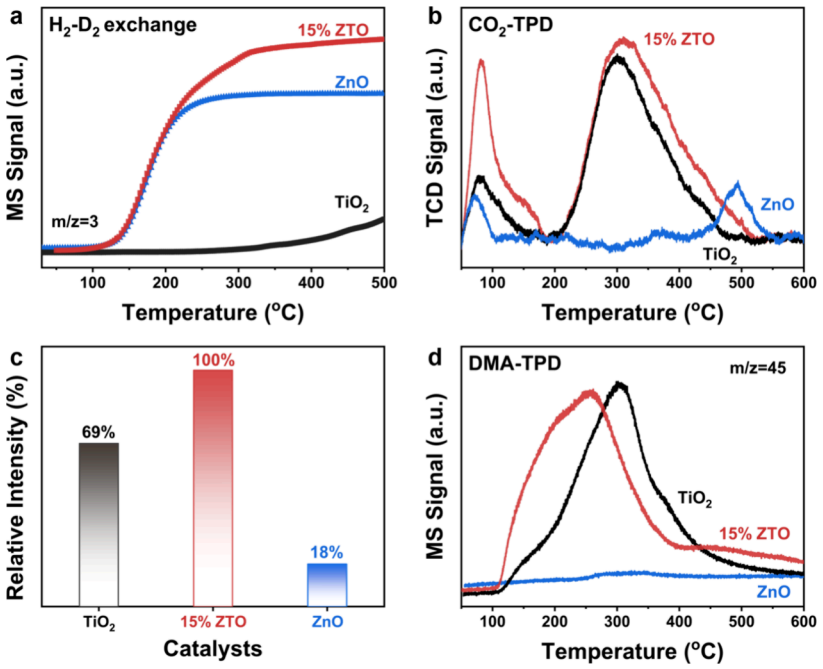

Figure 3. (a) H_2-D_2 exchange on ZnO, TiO_2, and 15% ZTO. (b) CO_2-TPD on ZnO, TiO_2, and 15% ZTO. (c) Mass-normalized relative intensity of CO_2 adsorption on ZnO, TiO_2, and 15% ZTO. (d) DMA-TPD on ZnO, TiO_2, and 15% ZTO.

at 742 cm^{-1}, characteristic of the $ZnTiO_3$ phase.[24] The Raman spectrum obtained with a 532 nm laser is dominated by peaks at 398, 520, and 639 cm^{-1} for TiO_2 and χ% ZTO (χ = 1, 5, 10, 15, 20, and 30), consistent with the anatase phase.[23] These results suggest that both the skin layer and bulk are in the anatase phase, further confirming the solid solution structure of 15% ZTO.

The transmission electron microscopy and aberration-corrected high-angle annular dark-field scanning transmission electron microscopy images clearly show the 15% ZTO nanoparticles with particle sizes of 20−50 nm (Figure 2c and Figure S8). The (101) interplanar spacing of 15% ZTO is 0.36 nm, which is wider than that of anatase TiO_2 due to the doping of Zn into TiO_2 (Figure 2c). Energy-dispersive spectroscopic elementary mappings of 15% ZTO particles indicate that Zn is uniformly dispersed in the TiO_2 matrix (Figure 2d). Formation of the Zn−O−Ti motif is verified by an atomic-resolution scanning transmission electron microscopy image and atomic intensity analysis, illustrating that Zn is successfully introduced into the lattice of TiO_2 to replace part of the Ti sites (Figure S9). The time-of-flight neutron powder diffraction patterns and Rietveld refinements further suggest that 15% ZTO consists of a $Zn_{0.15}Ti_{0.85}O_{1.85}$ solid solution, which shows anatase phases (Figure 2e and Table S3). Zn K-edge X-ray absorption spectroscopy was used to determine the local coordination environment of 15% ZTO (Figures S10−S12). Compared with ZnO and Zn foil reference compounds, the Zn K-edge X-ray absorption near-edge spectroscopy (XANES) spectra show that the valence state of Zn in χ% ZTO (χ = 5, 10, and 30) is higher than that in ZnO, and the Zn species in these three ZTO samples exhibit the same valence state (Figure 2f), indicating that electrons from Zn species in ZTO transfer to the Ti species. These results align well with the conclusion drawn from the X-ray photoelectron spectroscopy (XPS) spectra of 15% ZTO (Figure S13). Figure 2g displays the radial structure functions (RSFs) of the samples and reference compounds. For ZnO and 15% ZTO, a peak at 1.6 Å appears, corresponding to the first-nearest neighbor Zn−O distance. The peak at 2.9 Å is related to the first- and second-nearest neighbor Zn−Zn distances in ZnO.[25] It is worth noting that the RSF of 5 and 15% ZTO does not have the Zn−Zn peak, indicating that the Zn species are isolated [−Zn−O−] species. Along with an increase in the Zn content to 30%, a weak Zn−Zn peak emerges, suggesting the formation of ZnO clusters or oligomers. The Zn coordination environment was further confirmed by wavelet transformation (Figure S12). XPS and inductively coupled plasma−atomic emission spectrometry analyses (Figure S14) confirm that the surface Zn concentration aligns with the theoretical Zn/(Zn + Ti) atomic ratio for values below 20%. As the Zn content increases, the surface Zn concentration slightly exceeds the theoretical value. These results indicate that the 15% ZTO catalyst is a solid solution in the phase transition from the skin layer to bulk, as schematically depicted in Figure 2h.

H_2 activation over these catalysts was investigated through H_2-D_2 isotope exchange experiments. Figure 3a shows that the initial temperatures for HD formation are about 130, 300, and 130 °C for ZnO, TiO_2, and 15% ZTO, respectively. ZnO and 15% ZTO display similar kinetic behavior, quickly reaching the thermodynamic equilibrium. However, TiO_2 exhibits sluggish kinetics for H_2-D_2 exchange experiments. This result reveals that, compared with TiO_2, ZnO shows a lower H_2 activation barrier, and doping ZnO into TiO_2 significantly enhances the ability of H_2 activation over 15% ZTO. Thus, it can be deduced that H_2 mainly activates on ZnO sites of 15% ZTO.

CO_2-TPD (temperature-programmed desorption of CO_2) of catalysts shows two desorption peaks. Both TiO_2 and 15% ZTO exhibit peaks centered at 100 and 320 °C, while ZnO shows peaks at 100 and 500 °C (Figure 3b). The total CO_2 adsorption amounts and the CO_2 adsorption capability below the reaction temperature for these catalysts are ranked as follows: 15% ZTO > TiO_2 > ZnO (Figure 3b,c). When normalized by specific surface area, the CO_2 adsorption amounts for these catalysts follow the order 15% ZTO > TiO_2

https://doi.org/10.1021/jacs.4c12503
J. Am. Chem. Soc. XXXX, XXX, XXX−XXX

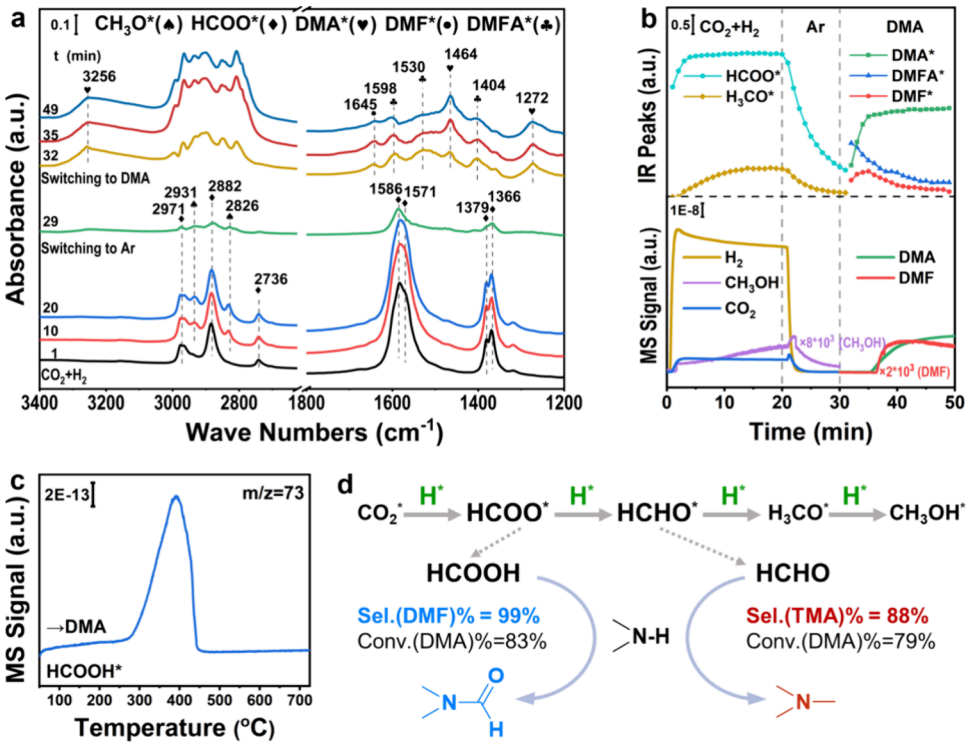

Figure 4. (a) *Operando* DRIFT spectra of surface species formed from the CO_2 + H_2 + DMA reaction on 15% ZTO. A mixture of 10 mL/min CO_2 and 30 mL/min H_2 was injected at 10−20 min, then switched to Ar at 21−29 min, and finally switched to DMA. (b) Intensities of the IR peaks and mass signals of surface species during process (a). Reaction conditions: 15% ZTO catalyst, 0.1 MPa, 300 °C, 10 mL/min CO_2, 30 mL/min H_2, and 5 mL/min DMA (in Ar). (c) Temperature-programmed surface reaction of HCOOH and DMA on 15% ZTO. (d) Scheme of surface species for DMF synthesis via CO_2 hydrogenation and the reaction results of DMA with HCOOH and CH_2O. Reaction conditions: 15% ZnO-TiO_2 catalyst, reaction with 3 MPa H_2 at 200 °C for 3 h.

> ZnO (Figures S15 and S16 and Table S2). These results suggest a strong synergistic effect between the Zn and Ti sites in 15% ZTO for CO_2 adsorption. This is further supported experimentally by the fact that the 15% ZTO catalyst exhibits much higher catalytic activity than the mechanically mixed ZnO + TiO_2 (15:85) mixture (Figure S3).

DMA-TPD (temperature-programmed desorption of DMA) of TiO_2 and 15% ZTO shows the broad peak centered at 300 °C, while ZnO hardly adsorbs DMA, indicating that DMA mainly adsorbs on Ti sites (Figure 3d). The CO_2-TPD and DMA-TPD results demonstrate that CO_2 adsorption involves the synergistic interaction between Zn and Ti sites, whereas DMA adsorption occurs primarily on the Ti sites. Temperature-programmed codesorption (TPD-co) of CO_2 and DMA was conducted by initially adsorbing DMA and then CO_2 over 15% ZTO (Figure S17). The DMA-TPD-co profile shows a broad peak centered at 300 °C, similar to the DMA-TPD results for 15% ZTO. The CO_2-TPD-co profile exhibits two peaks centered at 100 and 350 °C, with a slight decrease in intensity at 350 °C compared to the CO_2-TPD results for 15% ZTO. These results suggest that the adsorption of DMA has a negligible influence on the adsorption of CO_2. Therefore, based on H_2-D_2 exchange reaction and TPD results, it can be concluded that H_2 activates over Zn sites, and DMA mainly activates on Ti sites, but the activation of CO_2 requires the synergistic Zn and Ti sites.

To elucidate the reaction mechanism of CO_2 hydrogenation coupling with DMA to DMF on the 15% ZTO catalyst, the surface species evolving during the reaction were monitored by using *operando* diffuse reflectance infrared Fourier transform spectroscopy (*operando* DRIFTS) combined with mass spectrometry (MS) (Figure 4a,b and Figures S18 and S19). When CO_2 and H_2 were fed over 15% ZTO, HCOO* and CH_3O* species were observed and identified (Figure 4a). The infrared (IR) peaks at 1586 and 1571 cm^{-1} correspond to the asymmetric OCO stretching vibrations of adsorbed bidentate HCOO* species (the magnification of peaks at 1586 and 1571 cm^{-1} is shown in Figure S19c), while the peak at 1366 cm^{-1} is attributed to symmetric OCO stretching vibrations[26−32] (Figure 4a and Figure S18). These findings indicate that the formate species are adsorbed on two different active sites of 15% ZTO: those adsorbed on −Zn−O−Ti− asymmetric sites (peak at 1586 cm^{-1}) and those on −Ti−O−Ti− symmetric sites (peak at 1571 cm^{-1})[32] (Figures S19 and S20). The peaks at 2882 and 1379 cm^{-1} are assigned to the stretching and bending vibrations of ν(CH) and δ(CH), respectively, and the peaks at 2931 and 2826 cm^{-1} are attributed to CH_3O* species.[26,27,31] The peaks at 2882 and 2826 cm^{-1} were used to monitor the concentration changes of the HCOO* and CH_3O* species over time (Figure 4b). Initially, the surface HCOO* reaches a steady state, followed by CH_3O* gradually achieving its steady state. When CO_2 and H_2 were replaced by Ar, the concentrations of the formed HCOO* and CH_3O* species decreased. The reaction products were detected by MS, revealing a methanol signal after monitoring the CH_3O* species. When Ar replaced CO_2 and H_2, the detectable methanol signal also decreased concurrently.

Introducing DMA into the reaction system resulted in the disappearance of the peaks at 1586, 1571, and 1366 cm^{-1} (assigned to HCOO* species),[26,28,31] and new peaks emerged

https://doi.org/10.1021/jacs.4c12503
J. Am. Chem. Soc. XXXX, XXX, XXX−XXX

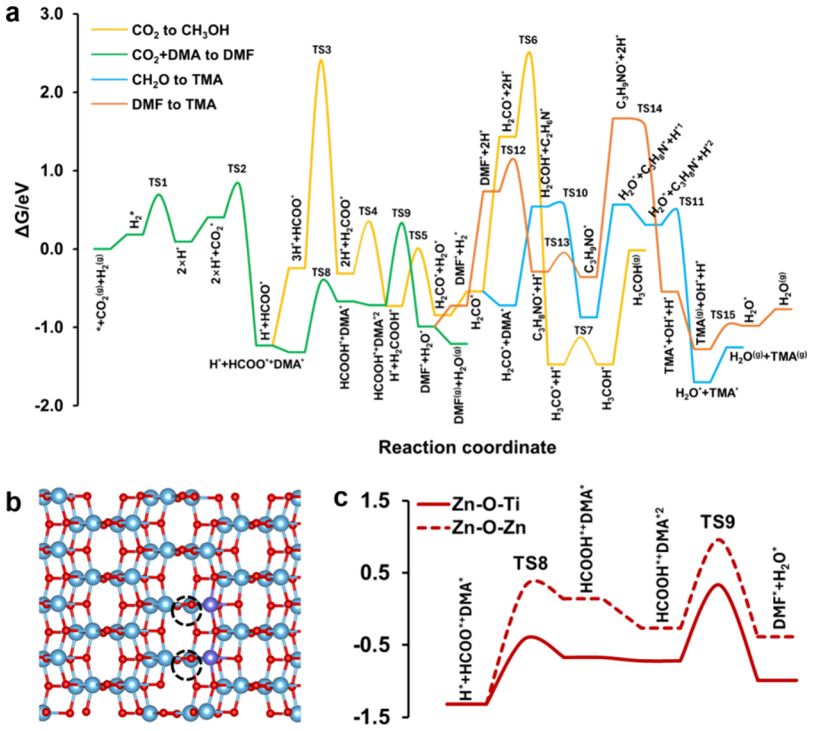

Figure 5. (a) Reaction diagram of four reaction pathways on the (101) surface of the tetragonal phase ZTO model (Gibbs free energy (G) is reported at a typical reaction temperature of 573 K). (b) Schematics of −Zn−O−Ti− and −Zn−O−Zn− motif distributions on the (101) surfaces of the tetragonal 15% ZTO catalysts (purple ball: Zn atom; cyan ball: Ti atom; red ball: O atom). (c) Free-energy diagrams of DMF production at 573 K on isolated −Zn−O−Ti− and −Zn−O−Zn− motifs.

(Figure 4a and Figure S19). The peaks at 1464 and 3256 cm^{-1} correspond to the N−H swinging and stretching vibrations of adsorbed DMA*, respectively, while the peak at 1530 cm^{-1} is associated with $N-H^+$ bending vibration, indicating a reaction between DMA* and HCOOH* to form $HCOO^-H_2N^+(CH_3)_2$ intermediates (DMFA*).[33] The peak at 1645 cm^{-1} corresponds to the C═O stretching vibration of adsorbed DMF*, indicating the formation of DMF* on the surface of 15% ZTO.[33] The peaks at 1272, 1404, and 1598 cm^{-1} are attributed to C−N stretching and C−H bending and asymmetric stretching vibrations of $-CH_3$, respectively.[33] The peaks at 1464, 1530, and 1645 cm^{-1} were used to monitor the concentration changes of DMA*, DMFA*, and DMF* species over time, respectively (Figure 4b). Upon introduction of DMA into the system, the concentration of DMA* species quickly reaches its maximum and then stabilizes. In the presence of DMA*, the surface formate species rapidly disappear, while the surface DMFA* species initially reach their maximum concentration before gradually decreasing. As the concentration of DMFA* species decreases, the DMF* species gradually attain their maximum concentration before decreasing, demonstrating that DMF* is derived from DMFA* species. DMF is monitored by MS after the maximum concentration of DMF* is reached. When DMA was introduced while maintaining CO_2/H_2, the peak at 1586 cm^{-1} attributed to formate species decreased, and the peak at 1530 cm^{-1} ascribed to DMFA* species appeared, gradually developed, and then remained stable (Figure S21), indicating a steady-state reaction on the surface in the presence of all reactants. *In situ* DRIFTS observation of 15% ZTO with an initial feed of HCOOH, followed by a switch to DMA, revealed the presence of DMA*, DMFA*, and DMF* species on the catalyst surface (Figure S22). The temperature-programmed surface reaction with initial adsorption of HCOOH followed by feeding DMA shows an obvious signal of DMF (Figure 4c). The reaction between HCOOH and DMA exhibits 98% selectivity for DMF under both H_2 and Ar atmospheres (Figure S23). These findings solidify the conclusion that the HCOOH* species is the key intermediate reacting with DMA for DMF synthesis via CO_2 hydrogenation.

To confirm HCOO* as the active intermediate species for CO_2 hydrogenation over 15% ZTO, isotope labeling experiments were conducted. The surface HCOO* and CH_3O* reach a steady state (Figure S24), and methanol is detectable by MS during CO_2 hydrogenation over 15% ZTO (Figure S25). Substituting CO_2 and H_2 with D_2 leads to a decrease in HCOO* and CH_3O*, while DCOO* and CH_2DO* initially increase followed by a subsequent decrease[27,31] (Figure S24). Methanol experiences a rapid decline, and D-substituted methanol is detected, reaching its maximum value before decreasing (Figure S25). These findings suggest that HCOO* and CH_3O* species serve as intermediates in the CO_2 hydrogenation on 15% ZTO. The absence of detectable methanol when DMA is introduced in CO_2 hydrogenation indicates that the reaction between HCOO* and DMA is much easier than the hydrogenation of HCOO* to methanol, and the HCOO* species is the intermediate for DMF synthesis.

TMA is the only byproduct for DMF synthesis via CO_2 hydrogenation. A previous study has reported that TMA formation can be ascribed to the subsequent hydrogenation of DMF over Cu-based catalysts.[20] 15% ZTO shows efficient activity for DMF synthesis with a TMA selectivity of only 1%. The reaction between HCOOH and DMA under H_2 results in a TMA selectivity of 2% over 15% ZTO (Figure S23). These results suggest that the formed DMF is relatively resistant to

https://doi.org/10.1021/jacs.4c12503
J. Am. Chem. Soc. XXXX, XXX, XXX−XXX

further hydrogenation to TMA over 15% ZTO. *Operando* DRIFTS and isotope labeling experiments indicate that formate and methoxy species are intermediates in methanol synthesis during CO_2 hydrogenation without DMA over 15% ZTO (Figures S24 and S25). Although CH_2O* species with high reaction activity are difficult to capture in CO_2 hydrogenation to methanol, it has been demonstrated that the CH_2O* species is the intermediate of HCOO* hydrogenation to CH_3O*. These findings are consistent with reported results for methanol synthesis via CO_2 hydrogenation over Cu-based,[26,28,34,35] ZnZrO,[31,32] and In_2O_3-based catalysts.[36−39] To determine whether CH_2O* serves as an intermediate in TMA production, the reaction between DMA with CH_2O was conducted, yielding TMA with an 88% selectivity (Figure S23). Based on these results, it is likely that the side-product TMA was produced through the reaction between DMA and the CH_2O* intermediate formed via the further hydrogenation of HCOO* over the 15% ZTO catalyst rather than through the hydrogenation of DMF.

Density functional theory (DFT) calculations were conducted to elucidate the reaction mechanisms (details in the Supporting Information), and the model for the ZnO-doped TiO_2 solid solution catalyst was constructed (Figure S26). Figure 5a illustrates the reaction energy diagram of four reaction pathways: CO_2 hydrogenation coupled with DMA to DMF, CO_2 hydrogenation to methanol, CO_2 hydrogenation coupled with DMA to TMA, and DMF hydrogenation to TMA on the surface of a ZnO-doped TiO_2 solid solution (detailed information in Figures S27−S30). H_2 is adsorbed and dissociated on the Zn site, while CO_2 and DMA initially adsorb on the coordination-unsaturated Ti sites in the proximity. The formation of the HCOO* species via CO_2* hydrogenation is energetically favorable, aligning with *operando* DRIFTS observations. DMF is produced through the dehydration between DMA* and HCOOH* species, a process confirmed to be favorable by DFT calculations ($\Delta G^{\#}$ = 1.05 eV; ΔG = −0.27 eV). In addition, the desorption of DMF* and H_2O* species from the 15% ZTO surface is facile.

The hydrogenation of HCOO* to H_2COO* displays the highest activation barrier of 2.65 eV along the CO_2 hydrogenation to methanol pathway, which is significantly higher than that of DMF synthesis. Subsequent hydrogenation of H_2COO* forms H_2COOH*, which undergoes C−O bond cleavage to generate H_2CO* and OH*. The conversion of H_2COO* to H_2CO* and H_2O* is thermodynamically unfavorable (ΔG = 0.66 eV). Although the reaction H_2CO* + H* → H_3CO* is exothermic (ΔG = −2.90 eV), H_2 dissociation over the Zn site in the presence of H_2CO* is difficult, resulting in an extremely high barrier for H_3CO* formation from H_2CO*. The H_3CO* species identified by theoretical calculation corresponds to the most stable reaction intermediate detected by *operando* DRIFTS. Finally, methanol is formed by H_3CO* protonation. Compared with CO_2 hydrogenation to methanol over 15% ZTO, DMF synthesis is more favorable both thermodynamically and kinetically. These findings are confirmed by experiments: methanol is undetectable in the presence of DMA during DMF synthesis via the hydrogenation of CO_2. Furthermore, 15% ZTO shows poor catalytic activity for CO_2 hydrogenation to methanol, with a CO_2 conversion of only 1.1% and a methanol selectivity of 90%. However, the CO_2 conversion has increased 2-fold for DMF synthesis via CO_2 hydrogenation. These results further demonstrate that the HCOO* species as the intermediate reacting with DMA for DMF synthesis is a favorable pathway, both thermodynamically and kinetically.

CO_2-TPD results have demonstrated that the synergistic effect between ZnO and TiO_2 significantly enhances CO_2 adsorption over 15% ZTO (Figure 3b,c). The experimental result indicates that, compared to 15% ZTO, the physical mixture of ZnO and TiO_2 shows lower activity for DMF synthesis (Figure S3). These findings suggest that the synergetic Zn and Ti sites facilitate the DMF synthesis. It has been demonstrated that formate species is the crucial intermediate reacting with DMA for DMF formation; meanwhile, the DRIFTS observations display the presence of formate species that adsorbed on asymmetrical −Zn−O−Ti− and symmetrical −Ti−O−Ti− sites. To understand the synergistic effect between Zn and Ti sites, −Zn−O−Zn− and −Zn−O−Ti− active motifs were constructed (Figure 5b). The formation process of HCOO* (Figure S28, TS8) and DMF* (Figure S28, TS9) species over −Zn−O−Zn− and −Zn−O−Ti− active motifs was investigated using DFT calculation. These steps were studied because the formation of HCOO* and DMF* species represents the highest reaction energy barrier for the DMF synthesis pathway (Figure 5c). Compared to −Zn−O−Zn− active sites, the synergistic −Zn−O−Ti− active sites facilitate the formation of HCOOH* and DMF* species, making their formation more favorable in both thermodynamics and kinetics. These results align with recent findings that formate species absorbed on asymmetric −Zn−O−Zr− sites are more easily converted to methanol through CO_2 hydrogenation compared to formate adsorbed on symmetric −Zr−O−Zr− sites.[31]

To elucidate the TMA formation pathway, both the reaction of DMA with CH_2O* and DMF hydrogenation were calculated and compared (Figure 5a). It is shown that C−N bond coupling between CH_2O* and DMA*, followed by consecutive hydrogenation to generate TMA*, is favorable with low activation barriers (Figure S29, TS10 and TS11). In contrast, the hydrogenation of DMF* ($(CH_3)_2NCHO$*) to intermediate C_3H_9NO* ($(CH_3)_2NCH_2OH$*) and subsequently to TMA* is difficult due to high activation barriers in kinetics and unfavorable thermodynamics (Figure S30, TS12 and TS14). Although the coupling of CH_2O* and DMA* for TMA synthesis is favorable both thermodynamically and kinetically, the formation of CH_2O* species through HCOO* hydrogenation is kinetically unfavorable compared to the reaction between DMA* and HCOO* for DMF synthesis over 15% ZTO. Therefore, the TMA formation occurs through the reaction of CH_2O* intermediates with DMA. However, due to sluggish kinetics for HCOO*-to-CH_2O* conversion, only a trace amount of TMA with a selectivity of 1% is produced. Based on the surface reaction kinetics and DFT calculation results, it is proposed that the DMF synthesis reaction via CO_2 hydrogenation coupled with DMA proceeds as follows: (1) generation of HCOO* via CO_2 hydrogenation on 15% ZTO, (2) reaction of HCOO* with DMA for DMF production, (3) formation of CH_2O* through further hydrogenation of HCOO* reacting with DMA for TMA production, and (4) the slow kinetics for HCOO* hydrogenation to CH_2O*, leading to low TMA selectivity.

The 15% ZTO catalyst displays substrate adaptability, facilitating the synthesis of *N*,*N*-diethylformamide (DEF) and *N*,*N*-dipropylformamide (DPF) through CO_2 hydrogenation coupled to diethylamine (DEA) and dipropylamine (DPA), respectively. The DEA and DPA conversions are 13 and 7%,

https://doi.org/10.1021/jacs.4c12503
J. Am. Chem. Soc. XXXX, XXX, XXX−XXX

respectively, and the selectivities for DEF and DPF reach up to 99% (Figure S31). This 15% ZTO catalyst, having undergone kilogram-scale amplification preparation, still upholds the superior performance of the originally prepared gram-scale catalyst (Figure S32). This substantiates the absence of any noticeable amplification effect in the preparation of the 15% ZTO catalyst.

CONCLUSIONS

This work demonstrates that binary metal oxide ZnO-TiO_2 in a solid solution state is a highly efficient catalyst for the synthesis of DMF through the hydrogenation of CO_2 coupled with DMA. The heterogeneous catalyst shows high selectivity and stability under industrial conditions. *Operando* DRIFTS results and DFT calculations reveal that the dual Zn and Ti sites on the ZnO-TiO_2 solid solution catalyst drive the efficient hydrogenation of CO_2 into formate species, which are pivotal intermediates that readily engage with DMA to form DMF. The high selectivity for DMF arises from the relatively slower kinetics of the formate hydrogenation to CH_2O* species, which suppresses the formation of the side-product TMA. By establishing a novel process for DMF synthesis utilizing key intermediates in CO_2 hydrogenation via heterogeneous catalysis with a fixed-bed reactor, this work makes large-scale DMF production practically feasible with the continuous flow reaction process.

ASSOCIATED CONTENT

Supporting Information

The Supporting Information is available free of charge at https://pubs.acs.org/doi/10.1021/jacs.4c12503.

Detailed experiment section, characterization methods, and DFT calculation methods (PDF)

AUTHOR INFORMATION

Corresponding Authors

Zelong Li − *Key Laboratory of Advanced Catalysis, Gansu Province, State Key Laboratory of Applied Organic Chemistry, College of Chemistry and Chemical Engineering, Lanzhou University, Lanzhou, Gansu 730000, China; State Key Laboratory for Oxo Synthesis and Selective Oxidation, Lanzhou Institute of Chemical Physics (LICP), Chinese Academy of Sciences, Lanzhou, Gansu 730000, China*; Email: lizl@lzu.edu.cn

Can Li − *Key Laboratory of Advanced Catalysis, Gansu Province, State Key Laboratory of Applied Organic Chemistry, College of Chemistry and Chemical Engineering, Lanzhou University, Lanzhou, Gansu 730000, China; Dalian National Laboratory for Clean Energy, State Key Laboratory of Catalysis, Dalian Institute of Chemical Physics, Chinese Academy of Sciences, Dalian, Liaoning 116023, China*; orcid.org/0000-0002-9301-7850; Email: canli@dicp.ac.cn

Authors

Jieyun Zhang − *Key Laboratory of Advanced Catalysis, Gansu Province, State Key Laboratory of Applied Organic Chemistry, College of Chemistry and Chemical Engineering, Lanzhou University, Lanzhou, Gansu 730000, China*

Guanna Li − *Biobased Chemistry and Technology Group, Wageningen University, 6708 WG Wageningen, The Netherlands*; orcid.org/0000-0003-3031-8119

Jin Xie − *Key Laboratory of Advanced Catalysis, Gansu Province, State Key Laboratory of Applied Organic Chemistry, College of Chemistry and Chemical Engineering, Lanzhou University, Lanzhou, Gansu 730000, China*

Yang Hai − *School of Mechanical Engineering, Dongguan University of Technology, Dongguan, Guangdong 523000, China*

Weiming Wan − *Key Laboratory of Advanced Catalysis, Gansu Province, State Key Laboratory of Applied Organic Chemistry, College of Chemistry and Chemical Engineering, Lanzhou University, Lanzhou, Gansu 730000, China*

Haotian Sun − *Key Laboratory of Advanced Catalysis, Gansu Province, State Key Laboratory of Applied Organic Chemistry, College of Chemistry and Chemical Engineering, Lanzhou University, Lanzhou, Gansu 730000, China*

Bin Wang − *Key Laboratory of Advanced Catalysis, Gansu Province, State Key Laboratory of Applied Organic Chemistry, College of Chemistry and Chemical Engineering, Lanzhou University, Lanzhou, Gansu 730000, China*

Xiaojing Wu − *Key Laboratory of Advanced Catalysis, Gansu Province, State Key Laboratory of Applied Organic Chemistry, College of Chemistry and Chemical Engineering, Lanzhou University, Lanzhou, Gansu 730000, China*

Jiannian Cheng − *Key Laboratory of Advanced Catalysis, Gansu Province, State Key Laboratory of Applied Organic Chemistry, College of Chemistry and Chemical Engineering, Lanzhou University, Lanzhou, Gansu 730000, China*

Changxin He − *Key Laboratory of Advanced Catalysis, Gansu Province, State Key Laboratory of Applied Organic Chemistry, College of Chemistry and Chemical Engineering, Lanzhou University, Lanzhou, Gansu 730000, China*

Wei Hu − *Key Laboratory of Advanced Catalysis, Gansu Province, State Key Laboratory of Applied Organic Chemistry, College of Chemistry and Chemical Engineering, Lanzhou University, Lanzhou, Gansu 730000, China*

Ying Zhang − *Dalian National Laboratory for Clean Energy, State Key Laboratory of Catalysis, Dalian Institute of Chemical Physics, Chinese Academy of Sciences, Dalian, Liaoning 116023, China*

Complete contact information is available at: https://pubs.acs.org/10.1021/jacs.4c12503

Author Contributions

‖J.Z. and G.L. contributed equally to this work.

Notes

The authors declare no competing financial interest.

ACKNOWLEDGMENTS

This work is supported the National Natural Science Foundation of China (grant nos. U24A20493 and 22072061).

REFERENCES

(1) Ding, S.; Jiao, N. N,N-Dimethylformamide: A Multipurpose Building Block. *Angew. Chem., Int. Ed. Engl.* **2012**, *51* (37), 9226−9237.

(2) Haynes, P.; Slaugh, L. H.; Kohnle, J. F. Formamides from carbon dioxide, amines and hydrogen in the presence of metal complexes. *Tetrahedron Lett.* **1970**, *11* (5), 365−368.

(3) Artz, J.; Müller, T. E.; Thenert, K.; Kleinekorte, J.; Meys, R.; Sternberg, A.; Bardow, A.; Leitner, W. Sustainable Conversion of Carbon Dioxide: An Integrated Review of Catalysis and Life Cycle Assessment. *Chem. Rev.* **2018**, *118* (2), 434−504.

(4) Liu, Q.; Wu, L.; Jackstell, R.; Beller, M. Using carbon dioxide as a building block in organic synthesis. *Nat. Commun.* **2015**, *6* (1), 5933.
(5) Jessop, P. G.; Hsiao, Y.; Ikariya, T.; Noyori, R. Homogeneous Catalysis in Supercritical Fluids: Hydrogenation of Supercritical Carbon Dioxide to Formic Acid, Alkyl Formates, and Formamides. *J. Am. Chem. Soc.* **1996**, *118* (2), 344−355.
(6) Kröcher, O.; Köppel, R. A.; Baiker, A. Highly active ruthenium complexes with bidentate phosphine ligands for the solvent-free catalytic synthesis of N,N-dimethylformamide and methyl formate. *Chem. Commun.* **1997**, *5*, 453−454.
(7) Kuhlmann, R.; Nowotny, M.; Künnemann, K. U.; Behr, A.; Vorholt, A. J. Identification of key mechanics in the ruthenium catalyzed synthesis of N,N-dimethylformamide from carbon dioxide in biphasic solvent systems. *J. Catal.* **2018**, *361*, 45−50.
(8) Shen, Y.; Zheng, Q.; Chen, Z.-N.; Wen, D.; Clark, J. H.; Xu, X.; Tu, T. Highly Efficient and Selective N-Formylation of Amines with CO_2 and H_2 Catalyzed by Porous Organometallic Polymers. *Angew. Chem., Int. Ed. Engl.* **2021**, *60* (8), 4125−4132.
(9) Zhang, L.; Han, Z.; Zhao, X.; Wang, Z.; Ding, K. Highly Efficient Ruthenium-Catalyzed N-Formylation of Amines with H_2 and CO_2. *Angew. Chem., Int. Ed. Engl.* **2015**, *54* (21), 6186−6189.
(10) Zhang, Y.; Wang, J.; Zhu, H.; Tu, T. N-Formylation of Amines with CO_2 and H_2 by Using NHC-Iridium Coordination Assemblies as Solid Molecular Catalysts. *Chem. - Asian J.* **2018**, *13* (20), 3018−3021.
(11) Daw, P.; Chakraborty, S.; Leitus, G.; Diskin-Posner, Y.; Ben-David, Y.; Milstein, D. SelectiveN-Formylation of Amines with H_2 and CO_2 Catalyzed by Cobalt Pincer Complexes. *ACS Catal.* **2017**, *7* (4), 2500−2504.
(12) Federsel, C.; Boddien, A.; Jackstell, R.; Jennerjahn, R.; Dyson, P. J.; Scopelliti, R.; Laurenczy, G.; Beller, M. A Well-Defined Iron Catalyst for the Reduction of Bicarbonates and Carbon Dioxide to Formates, Alkyl Formates, and Formamides. *Angew. Chem., Int. Ed. Engl.* **2010**, *49* (50), 9777−9780.
(13) Ziebart, C.; Federsel, C.; Anbarasan, P.; Jackstell, R.; Baumann, W.; Spannenberg, A.; Beller, M. Well-Defined Iron Catalyst for Improved Hydrogenation of Carbon Dioxide and Bicarbonate. *J. Am. Chem. Soc.* **2012**, *134* (51), 20701−20704.
(14) Cui, X.; Zhang, Y.; Deng, Y.; Shi, F. Amine formylation via carbon dioxide recycling catalyzed by a simple and efficient heterogeneous palladium catalyst. *Chem. Commun.* **2014**, *50* (2), 189−191.
(15) Dai, X.; Wang, B.; Wang, A.; Shi, F. Amine formylation with CO_2 and H_2 catalyzed by heterogeneous Pd/PAL catalyst. *China. J. Catal.* **2019**, *40* (8), 1141−1146.
(16) Zhang, Y.; Wang, H.; Yuan, H.; Shi, F. Hydroxyl Group-Regulated Active Nano-Pd/C Catalyst Generation via in Situ Reduction of Pd(NH_3)xCly/C for N-Formylation of Amines with CO_2/H_2. *ACS Sustainable Chem. Eng.* **2017**, *5* (7), 5758−5765.
(17) Bi, Q.-Y.; Lin, J.-D.; Liu, Y.-M.; Xie, S.-H.; He, H.-Y.; Cao, Y. Partially reduced iridium oxide clusters dispersed on titania as efficient catalysts for facile synthesis of dimethylformamide from CO_2, H_2 and dimethylamine. *Chem. Commun.* **2014**, *50* (65), 9138−9140.
(18) Wang, G.; Jiang, M.; Ji, G.; Sun, Z.; Li, C.; Yan, L.; Ding, Y. Bifunctional Heterogeneous Ru/POP Catalyst Embedded with Alkali for the N-Formylation of Amine and CO_2. *ACS Sustainable Chem. Eng.* **2020**, *8* (14), 5576−5583.
(19) Liu, J.; Guo, C.; Zhang, Z.; Jiang, T.; Liu, H.; Song, J.; Fan, H.; Han, B. Synthesis of dimethylformamide from CO_2, H_2 and dimethylamine over Cu/ZnO. *Chem. Commun.* **2010**, *46* (31), 5770−5772.
(20) Wu, Y.; Wang, T.; Wang, H.; Wang, X.; Dai, X.; Shi, F. Active catalyst construction for CO_2 recycling via catalytic synthesis of N-doped carbon on supported Cu. *Nat. Commun.* **2019**, *10*, 2599.
(21) Dai, X.; Li, T.; Wang, B.; Kreyenschulte, C.; Bartling, S.; Liu, S.; He, D.; Yuan, H.; Brückner, A.; Shi, F.; Rabeah, J.; Cui, X. Tailoring Active Cu_2O/Copper Interface Sites for N-Formylation of Aliphatic Primary Amines with CO_2/H_2. *Angew. Chem., Int. Ed. Engl.* **2023**, *62* (21), No. e202217380.
(22) Wu, J.; Saito, M.; Takeuchi, M.; Watanabe, T. The stability of Cu/ZnO-based catalysts in methanol synthesis from a CO_2-rich feed and from a CO-rich feed. *Appl. Catal. A-Gen.* **2001**, *218* (1), 235−240.
(23) Choi, H. C.; Jung, Y. M.; Kim, S. B. Size effects in the Raman spectra of TiO_2 nanoparticles. *Vib. Spectroscopy* **2005**, *37* (1), 33−38.
(24) Bernert, T.; Ruiz-Fuertes, J.; Bayarjargal, L.; Winkler, B. Synthesis and high (pressure, temperature) stability of $ZnTiO_3$ polymorphs studied by Raman spectroscopy. *Solid State Sci.* **2015**, *43*, 53−58.
(25) Tada, S.; Ochiai, N.; Kinoshita, H.; Yoshida, M.; Shimada, N.; Joutsuka, T.; Nishijima, M.; Honma, T.; Yamauchi, N.; Kobayashi, Y.; Iyoki, K. Active Sites on $Zn_xZr_{1-x}O_{2-x}$ Solid Solution Catalysts for CO_2-to-Methanol Hydrogenation. *ACS Catal.* **2022**, *12*, 7748−7759.
(26) Kattel, S.; Yan, B.; Yang, Y.; Chen, J. G.; Liu, P. Optimizing Binding Energies of Key Intermediates for CO_2 Hydrogenation to Methanol over Oxide-Supported Copper. *J. Am. Chem. Soc.* **2016**, *138* (38), 12440−12450.
(27) Shido, T.; Iwasawa, Y. The Effect of Coadsorbates in Reverse Water-Gas Shift Reaction on ZnO, in Relation to Reactant-Promoted Reaction Mechanism. *J. Catal.* **1993**, *140* (2), 575−584.
(28) Zabilskiy, M.; Sushkevich, V. L.; Palagin, D.; Newton, M. A.; Krumeich, F.; van Bokhoven, J. A. The unique interplay between copper and zinc during catalytic carbon dioxide hydrogenation to methanol. *Nat. Commun.* **2020**, *11*, 2409.
(29) He, M.-Y.; White, J. M.; Ekerdt, J. G. CO and CO_2 hydrogenation over metal oxides: a comparison of ZnO, TiO_2 and ZrO_2. *J. Mol. Catal.* **1985**, *30* (3), 415−430.
(30) Bando, K. K.; Sayama, K.; Kusama, H.; Okabe, K.; Arakawa, H. In-situ FT-IR study on CO_2 hydrogenation over Cu catalysts supported on SiO_2, Al_2O_3, and TiO_2. *Appl. Catal. A-Gen.* **1997**, *165* (1), 391−409.
(31) Wang, J.; Li, G.; Li, Z.; Tang, C.; Feng, Z.; An, H.; Liu, H.; Liu, T.; Li, C. A highly selective and stable ZnO-ZrO_2 solid solution catalyst for CO_2 hydrogenation to methanol. *Sci. Adv.* **2017**, *3* (10), No. e1701290.
(32) Feng, Z.; Tang, C.; Zhang, P.; Li, K.; Li, G.; Wang, J.; Feng, Z.; Li, C. Asymmetric Sites on the ZnZrOx Catalyst for Promoting Formate Formation and Transformation in CO_2 Hydrogenation. *J. Am. Chem. Soc.* **2023**, *145* (23), 12663−12672.
(33) Socrates, G. *Infrared and Raman characteristic group frequencies: tables and charts pbk.* 3rd ed.; J. Wiley: 2001.
(34) Kattel, S.; Ramírez, P. J.; Chen, J. G.; Rodriguez, J. A.; Liu, P. Active sites for CO_2 hydrogenation to methanol on Cu/ZnO catalysts. *Science* **2017**, *355* (6331), 1296−1299.
(35) Larmier, K.; Liao, W. C.; Tada, S.; Lam, E.; Verel, R.; Bansode, A.; Urakawa, A.; Comas-Vives, A.; Coperet, C. CO_2-to-Methanol Hydrogenation on Zirconia-Supported Copper Nanoparticles: Reaction Intermediates and the Role of the Metal-Support Interface. *Angew. Chem., Int. Ed. Engl.* **2017**, *56* (9), 2318−2323.
(36) Frei, M. S.; Capdevila-Cortada, M.; García-Muelas, R.; Mondelli, C.; López, N.; Stewart, J. A.; Curulla Ferré, D.; Pérez-Ramírez, J. Mechanism and Microkinetics of Methanol Synthesis via CO_2 Hydrogenation on Indium Oxide. *J. Catal.* **2018**, *361*, 313.
(37) Martin, O.; Martin, A. J.; Mondelli, C.; Mitchell, S.; Segawa, T. F.; Hauert, R.; Drouilly, C.; Curulla-Ferre, D.; Perez-Ramirez, J. Indium Oxide as a Superior Catalyst for Methanol Synthesis by CO_2 Hydrogenation. *Angew. Chem., Int. Ed. Engl.* **2016**, *55* (21), 6261−5.
(38) Ye, J.; Liu, C.; Mei, D.; Ge, Q. Active Oxygen Vacancy Site for Methanol Synthesis from CO_2 Hydrogenation on In2O3(110): A DFT Study. *ACS Catal.* **2013**, *3* (6), 1296−1306.
(39) Pinheiro Araújo, T.; Mondelli, C.; Agrachev, M.; Zou, T.; Willi, P. O.; Engel, K. M.; Grass, R. N.; Stark, W. J.; Safonova, O. V.; Jeschke, G.; Mitchell, S.; Pérez-Ramírez, J. Flame-made ternary Pd-In_2O_3-ZrO_2 catalyst with enhanced oxygen vacancy generation for CO_2 hydrogenation to methanol. *Nat. Commun.* **2022**, *13*, 5610.

https://doi.org/10.1021/jacs.4c12503
J. Am. Chem. Soc. XXXX, XXX, XXX−XXX